INSTITUTE OF PHYSICS PUBLISHING JOURNAL OF OPTICS A: PURE AND APPLIED OPTICS
J. Opt. A: Pure Appl. Opt. **4** (2002) 1–7 PII: S1464-4258(02)25520-8

Iterative reconstruction of thermally induced phase distortion in a Nd^{3+}:YVO_4 laser

Ludovic Grossard, Agnès Desfarges-Berthelemot, Bernard Colombeau and Claude Froehly

Institut de Recherche en Communications Optiques et Microondes, 123, avenue Albert Thomas, 87060 Limoges cedex, France

E-mail: grossard@ircom.unilim.fr

Received 6 June 2001, in final form 25 September 2001
Published 6 November 2001
Online at stacks.iop.org/JOptA/4/1

Abstract
The thermal distortions in a continuous-wave end-pumped Nd:YVO_4 laser are experimentally investigated by use of an external TEM_{00} probe beam (TEM standing for transverse electric magnetic). After a round-trip of this probe through the active medium, three irradiance profiles are recorded along its propagation axis. The distorted phase pattern of this probe beam is then reconstructed from these profiles by means of a Gerchberg–Saxton-like iterative algorithm. To identify the contribution of each kind of aberration in the phase profile, we have computed a Zernike polynomial expansion, and have shown that the main terms constituting the aberration are (in order) defocusing (optical path difference (OPD) 0.7 λ FWHM (full width at half-maximum)), spherical aberration (OPD 0.3 λ FWHM), and first-order astigmatism (OPD of $\pm 0.14\,\lambda_p$ FWHM). Moreover, all higher-order terms result in a significant phase peak (λ/4 FWHM over 400 μm).

Keywords: Solid-state laser, thermal distortions, diode-pumping, phase retrieval algorithm

1. Introduction

During the last few years, the use of end-pumped solid-state lasers has rapidly expanded partly because of their high conversion efficiency, easy transverse mode selection due to gain distribution inside the amplifying medium, and much appreciated ease of use. Moreover, the good spatial overlap between the pump and laser beams, on one hand, and the spectral matching between the pump beam wavelength and laser crystal absorption bandwidth, on the other hand, have strongly reduced thermal effects in the active medium. However, with higher diode power recently becoming available, thermal effects have again come to impose a serious limitation on the laser brightness, leading to either a multimodal emission or severe power losses if a TEM_{00} laser beam is maintained by intracavity filtering.

Wavefront aberrations can be corrected in real time using a phase conjugation technique based on four-wave mixing for example [1, 2]. However, this process induces a dramatic fall in global efficiency because of the high-power pump beam requirement. If the thermal distortions are time independent, the phase compensation can be performed in a static way. The thermal aberration reduction can be obtained for example by longitudinally cooling the amplifying medium [3], by designing a resonator geometry in which the laser beam size in the active medium is much smaller than the pump beam size [4], but the corresponding efficiency is low. The phase correction can also be achieved with a well-suited rectifying phase plate inserted in the cavity [5]. In the latter case, the thermal aberration could be entirely corrected if it is fully characterized.

Such a characterization has been performed for a CW end-pumped Nd:YAG laser by means of an interferometric device [4].

In this paper, we present a determination of the thermal effect in an end-pumped CW Nd:YVO_4 laser with a non-interferometric method where the distorted phase profiles are calculated by means of an iterative reconstruction process

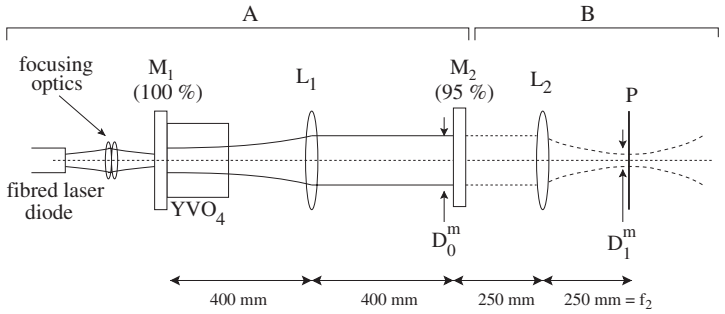

Figure 1. A: the laser studied for the characterization of thermal effects. B: the divergence parameter measurement.

using irradiance records. Such a technique has been previously used in stellar imaging to determine the Hubble Space Telescope wavefront distortions [6], and here, for the first time to our knowledge, this method is applied to measure the thermal effects in a running laser.

Firstly, we show experimentally that high pumping power leads to a spatially multimodal regime without any intracavity spatial filtering, indicating the need for an external TEM_{00} probe beam. Then, we present the probe beam distortion measurements when the pumping power is equal to 9 W. After a round-trip in the amplifying medium, irradiance profiles of this probe beam are recorded in several planes along its propagation axis. At least two planes are required [7] to reconstruct the optical field from irradiance measurements. However, using only two Fourier-transform planes, we did not recover the measured irradiance patterns from the reconstructed wavefront. That is why we used the irradiance profile in a third plane. Experimentally, the planes considered were the image of the active-medium output plane, its Fourier-transform plane, and a Fresnel one. The distorted wavefront is then reconstructed by means of an iterative Gerchberg–Saxton-like algorithm [7] using the three preceding irradiance measurements. Finally, the calculated phase profile in the laser crystal output plane is analysed using a Zernike polynomial expansion and the main aberration terms are pointed out.

2. Wavefront distortion measurement method

2.1. Laser wavefront distortion and beam divergence

The laser studied here is represented in figure 1. A 3 mm thick 1.1% Nd^{3+}:YVO_4 crystal is longitudinally end-pumped by a CW pigtailed laser diode at 808 nm. The active medium is birefringent and the laser beam is linearly polarized along the extraordinary axis. The mirror M_1 is totally reflecting for the laser line and anti-reflection coated at 808 nm. The power reflectance of the second mirror M_2 is equal to 95%. The two mirrors are located in the focal planes of a converging lens L_1 whose focal length is equal to 400 mm. This resonator is known as a Fourier-transform cavity.

Near the threshold, a TEM_{00} beam is emitted due to tri-dimensional gain filtering in the laser medium without additional spatial filtering by any aperture. If the pumping power is increased, the energy deposited in the laser crystal leads to a well-known thermal lens effect. Without any precautions, the laser mode fits to the aberration medium so that the wavefronts remain plane in the mirror planes. This leads to an increased beam divergence. It can be estimated from the measurements of the laser beam width (FWHM) D_0^m in the plane of mirror M_2 and the laser beam width (FWHM) D_1^m in the focal plane P of the lens L_2 ($f_2 = 250$ mm). With a TEM_{00} beam having a diameter equal to D_0^m in the plane of M_2, the calculated beam diameter D_1^c is equal to $2(\ln 2)\lambda f_2/\pi D_0^m$ in the plane P. We defined the ratio $k = D_1^m/D_1^c$ as a measurement of divergence.

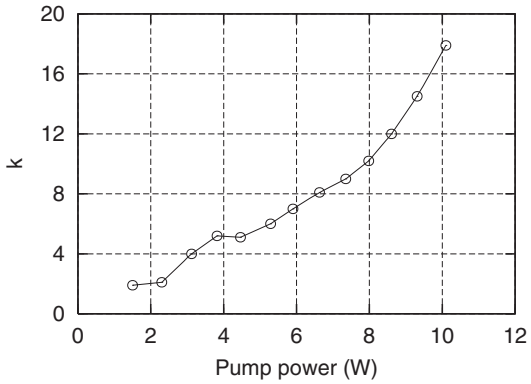

Figure 2. Divergence parameter of the laser beam versus the pumping power: $k = \pi D_0^m D_1^m/[2(\ln 2)\lambda f_2]$.

We observed (figure 2) that the divergence parameter k quickly increases from 1 near the threshold to about 18 at 9.7 W pumping. This means that near the threshold, the laser beam can be considered as diffraction limited, whereas under strong pumping power, the beam size D_1^m is 18 times what it should be if the beam profile was monomode. Under pumping power equal to 9.7 W, thermal lens effects result not in a fall in efficiency, but in a deterioration of the laser beam spatial quality, leading to a strong decrease in brightness. A TEM_{00} beam profile can be maintained by placing a spatial filter in the resonator, but the laser efficiency decreases because of important losses due to filtering.

2.2. External probe of wavefront distortions

When the pumping power is increased, the phase pattern of the laser beam is complicated because of the multimodal emission. This modal structure arises from the thermal distortion effects, on one hand, and from the plane-wavefront requirement for the resonator mirrors, on the other hand. It is therefore impossible to determine the thermally-induced index pattern in the amplifying medium by analysing the laser beam itself. A solution

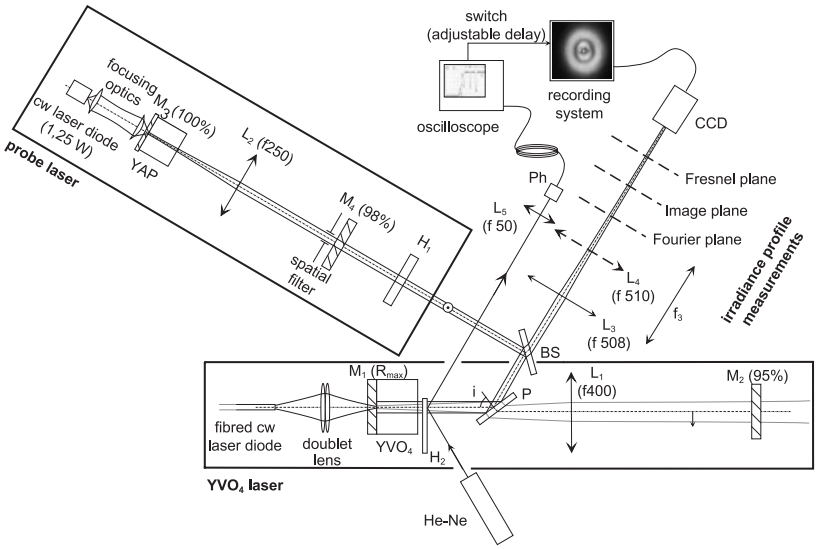

Figure 3. The experimental set-up used for the characterization of the thermal effects in an end-pumped YVO_4 laser. M_1, M_2, M_3, M_4: mirrors; L_1, L_2, L_3, L_4, L_5: lenses; P: polarizing plate; BS: beamsplitter; Ph: photodiode; H_1, H_2: half-wave plates. The image plane is obtained with the L_3 and L_4 lenses whereas the Fourier and Fresnel planes are obtained with the L_3 lens only.

consists in using an external probe plane wave and analysing its wavefront distortions after a round-trip in the amplifying medium. The distorted phase profile of the probe wave can be classically determined by interferometry. Here, we have developed an alternative method where this profile is calculated by means of three irradiance profile records of the probe beam using a Gerchberg–Saxton-like phase-retrieval algorithm.

3. Experimental set-up

The experimental set-up is shown in figure 3. This arrangement is divided into three parts: the probe YAP laser, the YVO_4 laser, and the irradiance measurement device.

3.1. Probe beam characteristics

The cavity of the probe laser is a Fourier-transform one, to give a laser beam with a large stability length. The active medium is a YAP:Nd^{3+} crystal pumped by a CW laser diode at 808 nm. The mirrors M_3 and M_4 are located in the focal planes of the lens L_2 (focal length 250 mm). A spatial filter is placed in the plane of mirror M_4 in order to obtain a high-spatial-quality TEM_{00} output laser beam. The probe beam wavelength is chosen equal to 1079 nm, i.e. outside the gain bandwidth of the YVO_4 crystal, to avoid modifications of the population inversion. However, this wavelength is close enough to the YVO_4 emission wavelength to limit chromatic dispersion effects. The probe beam is linearly polarized, and its direction of polarization is adjusted by a half-wave plate H_1 located outside the resonator.

The probe beam size near mirror M_4 is equal to 1 mm (FWHM), corresponding to a Rayleigh length of about 3 m. As the distance between the mirror M_4 and the YVO_4 crystal is approximately equal to 1.5 m, the field curvature of the probe beam in the crystal is not significant. This ensures that the YVO_4 crystal is probed by a quasi-plane-limited wavefront and that the reconstructed phase profile will not be affected by the intrinsic curvature of the probe beam.

3.2. Polarization requirements

The index changes versus temperature in the YVO_4 crystal are different along the ordinary and extraordinary axes, and therefore the probe beam and laser beam must have the same polarization in the laser medium. Under this condition, the probe beam injection leads to dramatic power losses for the YVO_4 laser. To overcome this problem, the laser emission is stopped when the amplifying medium is probed. The measurements are synchronized with the laser shutdown to avoid crystal warm-up because of non-radiative transitions. The probe beam injection is performed using the polarizing plate P inserted into the cavity. This plate is at Brewster incidence with the laser axis and is totally reflecting for the vertical polarization and AR coated for the horizontal one. The probe beam is then horizontally polarized by rotating the half-wave plate H_1 and the laser beam is horizontally polarized.

For the laser shutdown and measurement triggering, we used the following arrangement. Firstly, the laser is running and thermal stability is achieved. The probe beam is directed into the vanadate crystal with vertical polarization (figure 4(*a*)). Secondly, a half-wave H_2 plate is inserted between the polarizing plate P and the YVO_4 crystal. The trace of the polarization plane on the H_2 plate surface bisects the angle between the axes of the plate, so the probe beam undergoes a 90° rotation and does a round-trip in the laser crystal with the same polarization as the laser beam. The laser does not work any longer because of losses added by the 'polarizing plate P + half-wave plate H_2' combination (figure 4(*b*)).

3.3. Measurement triggering

The synchronization is obtained by use of an He–Ne laser beam and a photodiode as shown in figure 3. This beam is focused on the photodiode Ph using a 50 mm focal length lens L_5. The half-wave plate H_2 is inserted into the laser by means of an electric motor and crosses the YVO_4 laser beam for about 1 ms. We used the reflection of the He–Ne laser

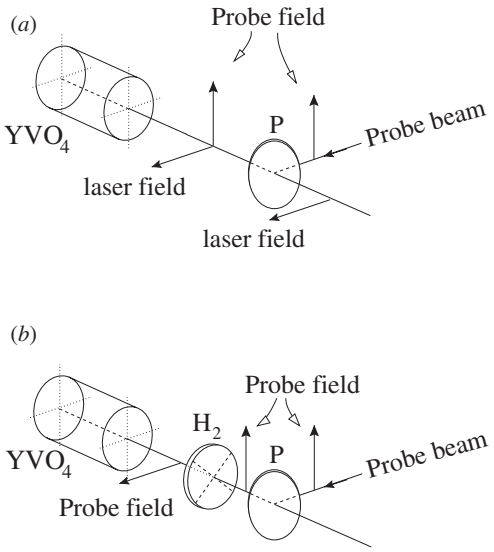

Figure 4. Probe beam injection method. P: polarizing plate; H_2: half-wave plate. (*a*) The laser is running and the probe field is vertically polarized. (*b*) H_2 is inserted into the resonator. The laser emission is shut down and the probe field is horizontally polarized. The measurements are performed as soon as possible to avoid crystal warm-up.

beam onto this plate to start the measurements. The voltage given by the resistor associated with the photodiode is used to trigger off an oscilloscope. A second signal is generated by the oscilloscope to activate the recording system, allowing us to add an adjustable delay.

3.4. Description of the irradiance measurement device

After a round-trip in the laser medium, the probe beam is partly transmitted through the beamsplitter BS, and defines the axis along which measurements of three irradiance patterns are performed:

- The first record is that of the image of the laser crystal output plane. This is obtained using two lenses L_3 and L_4, whose focal lengths are respectively equal to 508 and 510 mm. These lenses are positioned such that the laser crystal output plane is located in the object plane of L_3, and a CCD camera is placed in the Fourier plane of L_4. The distance between the two lenses is equal to 116 mm.
- Secondly, we record the irradiance of a field pattern which is a Fourier transform of the previous one. We simply removed L_4 and placed the camera in the Fourier plane of L_3.
- The third irradiance pattern is recorded in a Fresnel plane obtained by moving the CCD camera away from the Fourier plane by 270 mm.

Irradiance patterns are recorded with a TM-745 CCD camera (Pulnix) whose pixel size is equal to 11 μm $\times$ 11 μm. The irradiance recorded by each pixel is coded with 256 grey levels.

4. Experimental results

4.1. Irradiance profiles

Irradiance profiles were recorded in the three previously defined planes (named hereafter: image, Fourier, and Fresnel planes). These measurements were performed using three different experimental configurations (figure 5):

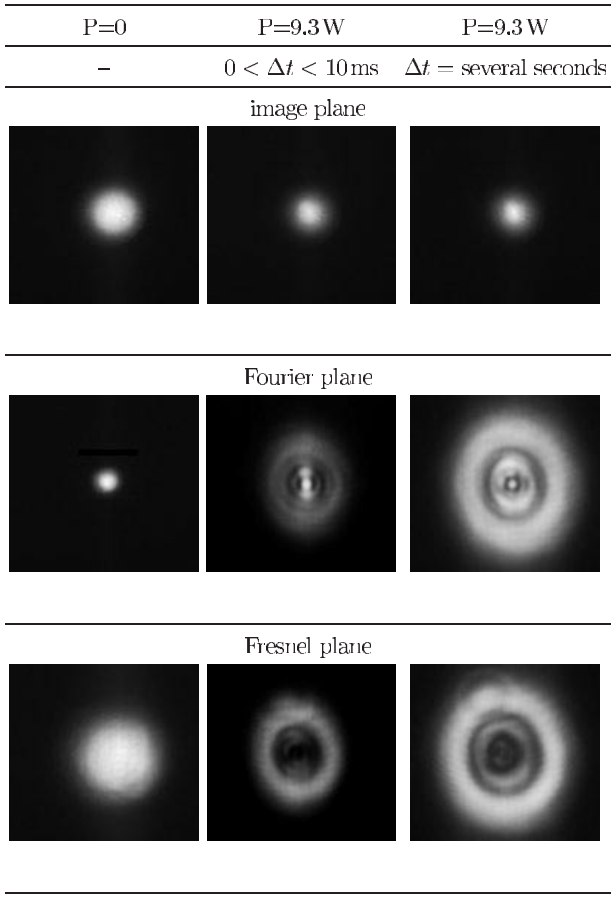

Figure 5. Measured irradiance profiles in the image, Fourier, and Fresnel planes. Column 1: pumping power $P = 0$ W. Column 2: $P = 9.3$ W and profiles recorded 10 ms after the laser shutdown. Column 3: $P = 9.3$ W and profiles recorded several seconds after the laser shutdown.

- The laser crystal is not pumped. This allows us to verify that the intrinsic phase curvature of the probe beam (i.e. only due to propagation) in the YVO_4 crystal is negligible.
- The pumping power is equal to 9.3 W. The irradiance profiles are recorded only some milliseconds after laser shutdown. These records will be further used to effectively determine the distorted phase profile.
- The pumping power is equal to 9.3 W. The irradiance profiles are recorded several seconds after laser shutdown in order to indicate the influence of the crystal warm-up when the pumping power is no longer removed by laser emission.

For each record, the probe beam power is adjusted to optimize the record dynamics. This explains why the profiles recorded several seconds after the laser shutdown seem brighter than those recorded only some milliseconds later: in fact, the total energy is the same for all profiles, but the distribution is not the same for each of them.

The elliptically observed irradiance distribution in the Fourier plane could be attributed to temperature gradient anisotropy and thermal stress in the amplifying medium, leading to an anisotropic index pattern.

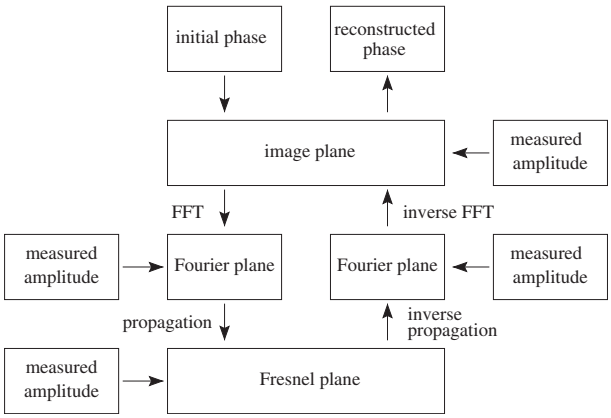

Figure 6. The numerical algorithm derived from the Gerchberg–Saxton algorithm and used for phase retrieval of the probe beam. The experimental data are amplitude profiles measured in three successive planes.

4.2. Phase-retrieval algorithm

The phase profile of the probe beam was determined using a Gerchberg–Saxton-like algorithm. This method allows us to reconstruct the distorted wavefront from a set of irradiance records along its propagation axis. A simplified version of the developed algorithm is shown in figure 6. Let us briefly discuss the various steps of this cyclic algorithm.

To begin, the phase profile in the image plane is set equal to zero as a first guess. The complex field in this plane is then constructed by multiplying this initial phase with the measured amplitude (which is proportional to the square root of the measured irradiance). This field undergoes a Fourier transform to give the complex field in the Fourier plane. The calculated amplitude is then removed and replaced by the measured one, while keeping the calculated phase profile unchanged. The complex field in the Fresnel plane is computed using the beam propagation method. Again, the calculated amplitude is replaced by the measured amplitude, while maintaining the calculated phase profile. This new complex field is then propagated back to the Fourier plane where the calculated amplitude is replaced again. An inverse Fourier transform operation gives the optic field in the initial plane, and so on.

The whole process is iterated until the calculated phase profile converges. After each iteration, the current error is estimated from the measured amplitude and from the reconstructed one in the Fourier plane. This error is calculated using the following expression:

$$\epsilon = \sqrt{\sum_{i,j} \left(I_2 - I_2^r\right)^2 \Big/ \left(\sum_{i,j} (I_2)^2\right)}$$

where I_2 and I_2^r denote the measured and reconstructed irradiance profiles in the Fourier plane. i and j are the coordinates of each pixel of the images. The convergence criterion is given by the current error stagnation.

Firstly, this algorithm was used to determine the intrinsic phase curvature of the probe beam in the laser crystal without thermal effects. Using the irradiance profiles obtained without a pump beam, we found an intrinsic phase curvature of the probe beam corresponding to an optical path difference (OPD) of $0.07\,\lambda_p$ (FWHM) where λ_p denotes the probe wavelength. Convergence of the algorithm was reached after only 20 iterations. Thus, this wavefront can be considered as a plane wave, and phase distortions of the probe beam under strong pumping conditions are directly linked to thermal aberrations.

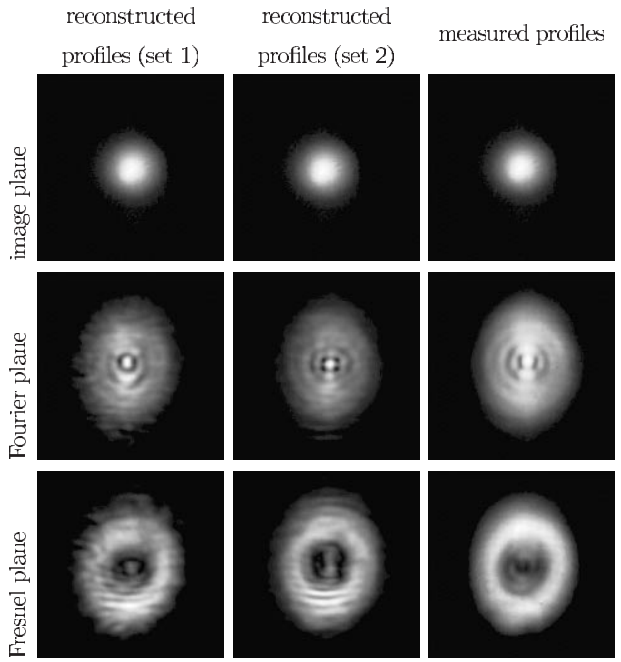

Figure 7. Reconstructed and measured irradiance profiles obtained with our algorithm in the image, Fourier, and Fresnel planes. Set 1: a plane wavefront as the initial condition in the image plane; set 2: a plane wavefront as the initial condition in the Fourier plane.

Secondly, the probe beam phase profile was reconstructed using irradiance profiles recorded while pumping the laser medium, 10 ms after the laser emission shutdown.

The reconstructed and measured irradiance profiles in the three working planes are shown in figure 7. The reconstructed ones were obtained after 63 iterations. Column 1 represents reconstructed profiles using a constant value (plane wavefront) for the initial phase in the image plane. To emphasize that the reconstructed beam profiles do not depend on initial conditions, we performed the cyclic computation again with the same initial phase, but in the Fourier plane (column 2). For comparison, the measured profiles are shown in column 3.

The reconstructed phase profile in the image plane and the corresponding irradiance profile are shown in figure 8. Only phase values corresponding to irradiances much greater than the recording noise should be taken into account.

To entirely characterize the thermal aberration, we propose to estimate the contribution of each kind of well known aberration by means of a Zernike polynomial expansion of the reconstructed phase profile [8].

4.3. Zernike polynomial expansion of the reconstructed phase profile

The well known Zernike polynomials are related to the classical aberrations and thus provide a convenient mathematical expression for the aberration content in a wavefront using familiar terms.

Table 1. Zernike polynomial expansion coefficients for the reconstructed phase profile in the image plane.

Number	n	m	Polynomial	Definition	A_{nm}
1	0	0	1	Piston	2.2694
2	1	0	$r\sin\theta$	Tilt Y	−0.0158
3	1	1	$r\cos\theta$	Tilt X	−0.1601
4	2	0	$r^2\sin(2\theta)$	1st-order astigmatism 45°	−0.2425
5	**2**	**1**	$\mathbf{2r^2-1}$	**Defocusing**	**−2.3337**
6	**2**	**2**	$\boldsymbol{r^2\cos(2\theta)}$	**1st-order astigmatism** 0°	**0.8494**
7	3	0	$r^3\sin(3\theta)$	Trefoil 30°	−0.0174
8	3	1	$(3r^3-2r)\sin(\theta)$	Coma Y	−0.0127
9	3	2	$(3r^3-2r)\cos(\theta)$	Coma X	0.1772
10	3	3	$r^3\cos(3\theta)$	Trefoil 0°	−0.0452
11	4	0	$r^4\sin(4\theta)$	Tetrafoil 22.5°	−0.0361
12	4	1	$(4r^4-3r^2)\sin(2\theta)$	2nd-order astigmatism 45°	−0.1538
13	**4**	**2**	$\mathbf{6r^4-2r^2-1}$	**Spherical aberration**	**1.2419**
14	**4**	**3**	$\boldsymbol{(4r^4-3r^2)\cos(2\theta)}$	**2nd-order astigmatism 0°**	**−0.3399**
15	4	4	$r^4\cos(4\theta)$	Tetrafoil 0°	−0.0829

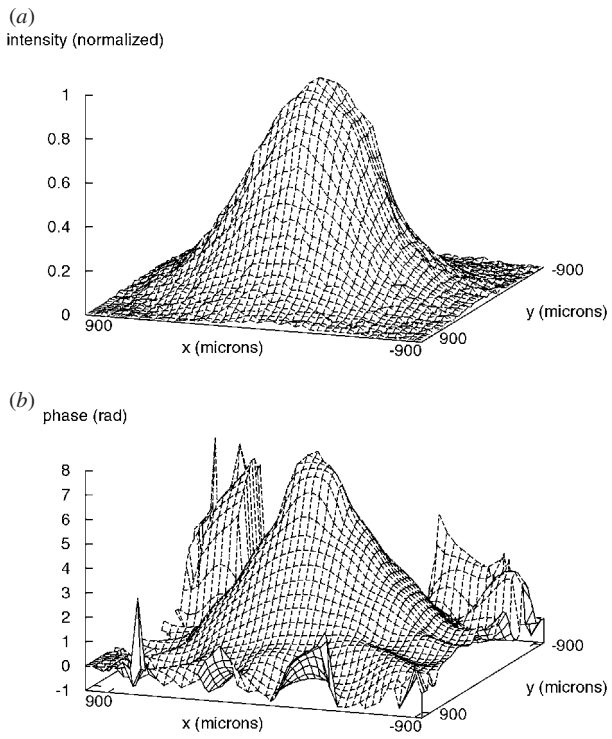

Figure 8. (*a*) The measured irradiance profile and (*b*) reconstructed phase profile in the image plane under strong thermal effects.

The Zernike polynomial expansion of the phase profile $\phi(\rho,\theta)$ is given by

$$\phi_1(\rho,\theta)=\sum_{n=0}^{k}\sum_{m=0}^{n}A_{nm}R_m^{n-2m}(\rho)\begin{cases}\sin(n-2m)\theta\\ \text{or}\\ \cos(n-2m)\theta\end{cases}$$

where the sine (cosine) function is used when $n-2m>0$ ($n-2m\leqslant 0$). A_{nm} are the coefficients of the expansion and $R_m^{n-2m}(\rho)$ denotes the Zernike polynomial. ρ and θ correspond to the polar coordinates.

Table 1 represents the first fifteen Zernike coefficients with the corresponding aberrations.

Three kinds of well known aberration were found to be significant:

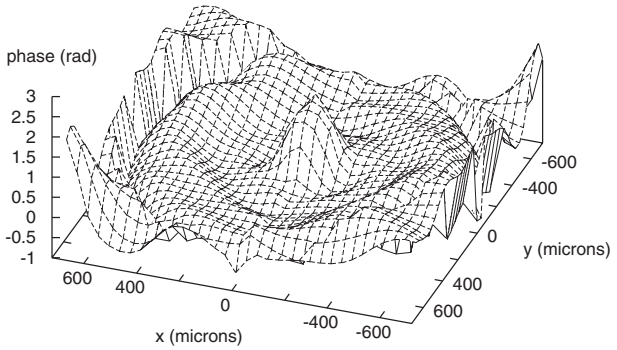

Figure 9. Phase distortion after defocusing, spherical aberration, and first-order astigmatism removal. This residual aberration is characterized by a $\lambda_p/4$ OPD (FWHM) over a 400 μm diameter.

- Defocusing (OPD of $0.7\,\lambda_p$ FWHM).
- Spherical aberration (OPD of $0.3\,\lambda_p$ FWHM).
- First-order astigmatism (OPD of $\pm 0.14\,\lambda_p$ (FWHM), the sign depending on the axis).
- Higher-order aberration: $\lambda_p/4$ curvature on 400 μm.

The distorted phase profile is mainly constituted by the parabolic term, due to the non-aberrant thermal lens. This phase contribution has no practical importance for further aberration compensation as it can be cancelled by simply translating the internal lens of the resonator.

It appears that spherical aberration and first-order astigmatism cannot be neglected compared to the parabolic term and should be taken into account to obtain an efficient phase correction. Moreover, the sum of all higher-order aberrations results in a significant phase curvature (OPD: $\lambda_p/4$ FWHM) over a 400 μm diameter as shown in figure 9. Such an aberration, leading to strong wavefront distortions after some round-trips in the laser resonator, should also be considered in the correction process.

5. Conclusions

To conclude, the effects of thermally induced index variation on a probe beam injected in a CW diode end-pumped YVO_4 laser have been characterized.

First of all, we showed experimentally that under strong pumping power, the beam profile becomes multimodal without additional intracavity filtering. Thus, the phase retrieval cannot be achieved by directly analysing the laser beam. That is why thermal effect measurements were performed using an external TEM_{00} probe beam. The emission wavelength of this probe ($\lambda_p = 1079$ nm) was chosen outside the YVO_4 ($\lambda = 1064$ nm) gain bandwidth in order to avoid a change of the population inversion. The probe and laser beams have parallel polarizations and the recordings were obtained a few milliseconds after the laser shutdown. In this case, the measured thermal distortions are roughly those of the running laser.

After a round-trip in the laser medium, the irradiance of the probe beam was recorded in the three wavefront planes: the image of the laser medium output plane, its Fourier-transform plane, and a Fresnel one.

We have developed a Gerchberg–Saxton-like numerical algorithm in order to reconstruct the phase profile of the distorted probe beam using irradiance measurements in three planes. The calculated phase pattern in the output plane of the laser crystal was analysed using a Zernike polynomial expansion. Three major aberration terms were pointed out: defocusing (OPD of $0.7\,\lambda_p$ FWHM), spherical aberration (OPD of $0.3\,\lambda_p$ FWHM), and first-order astigmatism (OPD of $\pm 0.14\,\lambda_p$ FWHM). However, the aberration composed of all higher-order terms was found to be significant ($\lambda_p/4$ OPD FWHM). These distortions are dramatically enhanced in CW operation because of the high quality factor of the resonator and the low gain. Therefore, the whole aberration, including all the higher-order terms, has to be taken into account in the phase distortion correction process.

References

[1] Brignon A, Loiseau L, Larat C, Huignard J P and Pocholle J P 1999 *Appl. Phys.* B **19** 159

[2] Mailis S, Hendricks J, Shepherd D P, Tropper A C, Moore N, Eason R W, Crofts G J, Trew M and Damzen J 1999 *Opt. Lett.* **24** 972

[3] Brauch U, Giesen A, Karszewski M, Stewen C and Voss A 1995 *Opt. Lett.* **20** 713

[4] Clarkson W A and Hanna D C 1998 *Resonator Design Considerations for Efficient Operation of Solid-State Lasers End-Pumped by High-Power Diode Bars* ed R Kossowsky *et al* (Dordrecht: Kluwer)

[5] Tidwell S C, Seamens J F, Bowers M S and Cousins A 1992 *IEEE J. Quantum Electron.* **28** 997

[6] Roddier C and Roddier F 1993 *Appl. Opt.* **32** 2992

[7] Gerchberg R W and Saxton W O 1972 *Optik (Stuttgart)* **35** 237

[8] Brunson D 1997 Source files for determination of Zernike polynomial expansion; webpage ftp://ftp.mathworks.com/pub/contrib/v5/physics/zernikes/